



Measurement of the Charge-Signed Rapidity Difference in $W\gamma$ Events

The DØ Collaboration

(Dated: October 28, 2006)

We present a preliminary measurement of the charge-signed rapidity difference in $W\gamma$ events in the final states with the W decaying into $e\nu$ and $\mu\nu$. The data were collected by the DØ detector at Fermilab's Tevatron $p\bar{p}$ collider operating at $\sqrt{s} = 1.96$ TeV and correspond to an integrated luminosity of approximately 900 pb^{-1} . The observed distribution agrees well with the Standard Model prediction and is indicative of the radiation amplitude zero, expected theoretically in the $W\gamma$ production.

I. INTRODUCTION

In the Standard Model, interference among the three tree-level diagrams involved in $W\gamma$ production, shown in Fig. 1, creates a zero in the center-of-mass angular distribution, θ^* , between the W and the direction of the incoming quarks. This zero is known as the radiation amplitude zero, and it occurs at:

$$\cos(\theta^*) = \pm \frac{1}{3}, \quad (1)$$

where the positive sign is for W^- and negative for W^+ . Direct measurement of θ^* is problematic: when the W decays into a charged lepton and a neutrino, a two-fold ambiguity is introduced in the W rapidity solutions due to the unknown longitudinal momentum of the neutrino (p_z). However, it has been demonstrated [1] that the radiation amplitude zero is evident in the charge-sign photon-lepton rapidity difference as a dip around:

$$\text{sign}(\ell)[y(\gamma) - y(\ell)] \approx -0.3, \quad (2)$$

$$\text{where } y = \frac{1}{2} \ln \left(\frac{E + p_z}{E - p_z} \right). \quad (3)$$

The Standard Model prediction of this distribution is shown in Fig. 2. Also shown in this figure is the overlay of an alternative hypothesis that represents a set of anomalous $WW\gamma$ couplings in which the magnetic dipole moment of the W is zero. This alternative model is of interest since $W\gamma$ production has features of magnetic dipole radiation and switching off the dipole moment is expected to have no radiation zero. For more information on the $WW\gamma$ couplings see [2]. For this analysis, the leptonic decays are examined and the charge-signed rapidity difference between the lepton and photon is directly measured.

A number of effects may obscure the dip. Photons radiated off of the final state lepton is one effect, because these events are not produced by one of three tree-level diagrams. To minimize the final state radiation, a threshold is imposed on the transverse mass of the lepton-photon-neutrino system, where the transverse mass is defined as:

$$M_{T3}^2(l\gamma; \cancel{E}_T) = \left((M_{l\gamma}^2 + |\mathbf{p}_T(\gamma) + \mathbf{p}_T(l)|^2)^{\frac{1}{2}} + \cancel{E}_T \right)^2 - |\mathbf{p}_T(\gamma) + \mathbf{p}_T(l) + \cancel{E}_T|^2, \quad (4)$$

and \mathbf{p}_T is the transverse momentum 3-vector. The dip is further obscured by next-to-leading order (NLO) processes which do not exhibit a radiation amplitude zero. For instance the process $qg \rightarrow W\gamma q$ does not exhibit a radiation zero. It has been shown [3] that the NLO corrections increase with center-of-mass energy, so although the effect is weak at the Tevatron, it will make analysis difficult at the Large Hadron Collider. Poor rapidity resolution will make the dip less apparent as will poorly estimated backgrounds. Processes that can contribute to backgrounds are the ones involving jets misidentified as photons, electrons misidentified as photons due to a lost track, $Z\gamma$, and $W\gamma \rightarrow \tau\nu\gamma$. Furthermore, anomalous $WW\gamma$ couplings may fill in the dip because their existence will either reduce or completely remove the interference between the three tree-level amplitudes (See Fig. 2). Thus, a measurement of the radiation amplitude zero provides a probe of the $WW\gamma$ couplings.

II. THE DØ DETECTOR AND DATA SAMPLE

The DØ detector is described in detail elsewhere [4]. It includes a central tracking system composed of a silicon microstrip tracker (SMT) and a central fiber tracker (CFT), both are located within a 2 T superconducting solenoidal magnet and are optimized for tracking and vertexing at pseudorapidities of $|\eta| < 2.5$ for the CFT and $|\eta| < 3.0$ for the SMT.

$$\eta = -\ln[\tan(\theta/2)], \quad (5)$$

where θ is measured with respect to the beam line. Forward and central preshower detectors are located just outside of the tracking volume and are constructed of several layers of extruded triangular scintillator strips. Three liquid argon and uranium calorimeters provide coverage out to $|\eta| \approx 4.2$: a central section covering out to approximately $|\eta| < 1.1$ and two endcap calorimeters with an approximate coverage of $1.5 < |\eta| < 4.2$. Beyond the calorimetry is a muon system consisting of tracking detectors, scintillation counters, and a 1.8 T toroid with coverage for $|\eta| < 2$. Luminosity is measured using scintillator arrays located in front of the endcap calorimeter cryostats, covering $2.7 < |\eta| < 4.4$. Trigger and data acquisition systems are designed to accommodate the high luminosities of Run II of the Tevatron.

The data were collected between October 2002 and November 2005. The integrated luminosities for the sample are 933 pb^{-1} and 878 pb^{-1} for the electron and muon channels, respectively.

TABLE I: Summary of estimated backgrounds and number of selected events.

	Muon Channel	Electron Channel
Luminosity	878 pb ⁻¹	933 pb ⁻¹
$W + \text{jet}$ Background Events	98 ± 12 (stat. + sys.)	148 ± 17 (stat. + sys.)
leX Background Events	6 ± 2 (stat. + sys.)	34 ± 4 (stat. + sys.)
$W\gamma \rightarrow \tau\nu\gamma$ Background Events	2.6 ± 0.4 (stat. + sys.)	1.7 ± 0.2 (stat. + sys.)
$Z\gamma \rightarrow \ell\ell\gamma$ Background Events	8 ± 1 (stat. + sys.)	-
Candidate Events	245	389
Expected Signal	130 ± 9	211 ± 14
Measured Signal	130 ± 18	205 ± 26
Measured Cross Section	3.21 ± 0.49 (stat. + sys.) ± 0.20 (lumi.) pb	
Times Branching Ratio	3.12 ± 0.49 (stat. + sys.) ± 0.19 (lumi.) pb	

III. EVENT SELECTION

Events that are consistent with $W\gamma$ where the W boson decays to an electron or a muon along with an associated photon are selected.

The $W(\mu\nu)$ events are collected using a suite of single-muon triggers. The muon is required to be isolated in the tracker and calorimeter and to be associated with a central track with p_T greater than 20 GeV/ c . The event is required to have missing transverse energy greater than 20 GeV and no additional tracks with $p_T > 15$ GeV/ c or additional medium quality muons.

The $W(e\nu)$ events are collected using a suite of single-electron triggers. The electron is required to be in the central or forward calorimeters ($|\eta| < 1.1$ or $1.5 < |\eta| < 2.5$) with $E_T > 25$ GeV. The electron must be isolated in the calorimeter, have a shower shape consistent with an electromagnetic object, and have an associated central track. The event is required to have missing transverse energy greater than 25 GeV.

The photon identification requirements are the same for both channels. The photon is required to be in the central or forward calorimeters ($|\eta| < 1.1$ or $1.5 < |\eta| < 2.5$) with $E_T > 7$ GeV. The photon must be isolated in the calorimeter and tracker, have a shower shape consistent with an electromagnetic object, and have an associated preshower cluster. The photon and lepton are required to be separated in $\eta - \phi$ space ($\Delta R = \sqrt{(\Delta\eta)^2 + (\Delta\phi)^2} > 0.7$), where ϕ is the azimuthal angle. To remove final state radiation which obscures the dip in the SM charge-sign rapidity difference, the three-body transverse mass is required to be greater than 110 GeV/ c^2 . For the electron channel, the W transverse mass must be greater than 50 GeV/ c^2 , this further reduces the effect of final state radiation. Furthermore, the electron channel has a significant background from Z decays where one of the electrons mimics a photon signature. To reduce this background a Z veto cut is applied to the two-body mass of the electron-photon system which must not be within 89-99 GeV. The value of the two-body mass window is optimized to minimize the fractional uncertainty on the measured signal and is not symmetric about the Z mass since the expected signal has significantly more events below the Z mass than above it. For both channels, the event is rejected if the difference in the z position of the lepton's track at the distance of closest approach and the primary vertex used for the missing transverse energy calculation is greater than 3 cm. This cut is required since the Monte Carlo does not model the mismeasured missing transverse energy that would result from the misplaced vertex.

The total number of selected candidate events is shown in Table I. Also shown in this table are the background and expected signal estimates. Contributions to the uncertainty on the expected number of signal events come from the cross section times branching ratio (3.21 ± 0.08 (PDF) pb), the luminosity (6.1%), and the acceptance and efficiencies which are delineated below. Note that both the cross section and the acceptances are measured with respect to $W\gamma$ events with photon $E_T > 7$ GeV, $\Delta R_{\ell\gamma} > 0.7$, and $M_{T^3}(\ell\gamma; \cancel{E}_T) > 90$ GeV/ c^2 .

IV. EFFICIENCIES AND ACCEPTANCES

The acceptance is defined as the probability for $W\gamma$ events to pass the geometric and kinematic requirements and is determined with Monte Carlo. The efficiency is defined as the probability for the electrons, muons, and photons that meet the acceptance requirements to be collected by the trigger, reconstructed, and pass additional quality requirements. The efficiencies are determined from $D\bar{O}$ data.

For the acceptance determination, a leading order (LO) Monte Carlo developed by Baur [5] is used. To take into account NLO effects, a K -factor is utilized. To make these events look more like actual data, Pythia [6] is used to determine the initial boost of the $W\gamma$ system which is applied to the LO Monte Carlo four-vectors. A parameterized

TABLE II: Summary of Acceptance and Efficiencies.

Cut	Muon Channel	Electron Channel
Acceptance	0.164 ± 0.006 (sys.)	0.143 ± 0.001 (sys.)
Lepton ID	0.722 ± 0.002 (stat. + sys.)	0.77 ± 0.06 (stat. + sys.)
Trigger	0.660 ± 0.002 (stat. + sys.)	0.976 ± 0.002 (stat. + sys.)
Photon Preselection	0.91 ± 0.03 (stat. + sys.)	0.89 ± 0.03 (stat. + sys.)
Photon ID	0.80 ± 0.02 (stat. + sys.)	0.78 ± 0.02 (stat. + sys.)
$Z\gamma$ Veto	0.87 ± 0.01 (sys.)	-
Δz	0.94 ± 0.01 (sys.)	0.94 ± 0.01 (sys.)
Combined	0.046 ± 0.003	0.071 ± 0.007

Monte Carlo is then used to smear the resulting four-vectors to take into account detector resolutions, particularly those which may alter the observed rapidity distribution.

Efficiencies for muons and electrons are found with large $Z \rightarrow e^+e^-$ or $Z \rightarrow \mu^+\mu^-$ samples in the data using a tag-and-probe method. The “tag” lepton must pass tight lepton selections, leaving the “probe” lepton as an unbiased sample for estimating the efficiency. The average efficiency of the electron identification for $W\gamma$ events is estimated to be 0.77 ± 0.06 (stat. + sys.). The average efficiency of the muon identification for $W\gamma$ events is estimated to be 0.722 ± 0.002 (stat. + sys.).

It is difficult to determine the efficiency for reconstructing the photon from the data. Therefore, the full GEANT Monte Carlo simulation of the DØ detector is used for this purpose. However, data are used to verify the efficiency of the isolation and EM-fraction requirements for low-energy photons where ambient energy in the calorimeter may be a significant effect. The $Z \rightarrow ee$ events are selected, and the ambient energy is measured in an isolated area between the electrons. The ambient energy compares well with what is measured in a similar study with the GEANT MC. The average efficiency for $W\gamma$ events of the isolation and EM fraction requirements are estimated to be 0.91 ± 0.03 (stat. + sys.) and 0.89 ± 0.03 (stat. + sys.) for the muon and electron channels respectively.

There is also a sizeable sample of radiative $Z\gamma$ events, where a photon is radiated off of one of the final state leptons and so the three-body mass ($M_{\ell\ell\gamma}$) should reconstruct to the Z mass, as shown in Fig. 3. The low-energy photon reconstruction efficiency does not match the GEANT prediction, possibly due to the veto on the track match and the preshower confirmation requirements. To correct for this, the GEANT MC is scaled to reproduce the data result. The radiative $Z\gamma$ photon E_T spectrum does not provide sufficient statistics above 25 GeV, so the reconstruction efficiency for photons with larger transverse energies are determined with GEANT and application of a scaling factor from the ratio of electron data/MC efficiencies. These efficiencies are calculated separately for the central calorimeter (CC) and the end cap calorimeters (EC). The average efficiency for $W\gamma$ events of the photon identification requirements are estimated to be 0.80 ± 0.02 (stat. + sys.) and 0.78 ± 0.02 (stat. + sys.) for the muon and electron channels respectively.

A summary of the overall $W\gamma$ acceptance and efficiencies is given in Table II.

V. BACKGROUNDS

The following processes can contribute background to the $W\gamma$ sample,

- W + jet where a jet is misidentified as a photon,
- “ leX ” meaning any process that produces a lepton, an electron, and missing transverse energy where the electron is misidentified as a photon due to the electron tracking inefficiency,
- $Z\gamma$ where one lepton from the Z is lost and missing transverse energy is generated by the lost lepton or a mismeasured jet,
- $W\gamma \rightarrow \tau\nu\gamma$.

The dominant background for both channels is from W + jet production. A data method is used to estimate this background, since Monte Carlo estimates are less reliable. In this method, a normalization sample of W + jet events is selected with the same selection criteria as the signal, except the photon identification is replaced with a requirement that there be a jet with a significant fraction of calorimeter energy in the electromagnetic layers. The normalization sample is then scaled by the jet misidentification ratio to obtain the background estimate.

To estimate the jet misidentification ratio, a multijet sample is used to calculate the ratio of jets with a significant fraction of calorimeter energy in the electromagnetic layers to those that pass the photon identification requirements.

This method uses the assumption that the ratio is the same for both the candidate sample and QCD events. The ratio is found as a function of E_T in ten bins of $|\eta|$.

At higher E_T , prompt photon production will contaminate the multijet sample. To compensate for this contamination two methods are used. In first the method, Monte Carlo purity estimates are used to subtract the prompt photon contribution. In the second method, the original data points are fitted with a functional form that includes an additional term to account for the prompt photon contamination. The systematic uncertainty for this ratio is taken as the difference between the two methods.

The leX background is estimated by removing the track isolation requirement from the photon candidate and by requiring that there be a matching track. The number of leX events that are misidentified as $W\gamma$ events are then estimated by using the known tracking inefficiencies.

The $Z\gamma$ and $W\gamma \rightarrow \tau\nu\gamma$ are estimated from Monte Carlo. A summary of the background estimates and observed $W\gamma$ candidate events is located in Table I.

VI. CHARGE MISIDENTIFICATION AND ASYMMETRY STUDIES

Charge misidentification would alter the charge-signed rapidity distribution. Hence, it is modeled in the Monte Carlo simulation. Charge misidentification for muons has been studied elsewhere [7] and for the selection criteria used here was shown to be $(1.62 \pm 0.04)\%$. For electrons, the charge misidentification was studied [8] and was shown to be $(1.0 \pm 0.5)\%$.

There is a concern that the detector fiducial acceptance and selection criteria may artificially introduce a rapidity asymmetry. As a check that this is not the case, $Z\gamma$ data events which have no intrinsic rapidity asymmetry are examined. The $Z\gamma$ events are made to resemble $W\gamma$ events by taking one of the leptons and treating it as a neutrino. The $Z\gamma$ events are selected using the $W\gamma$ selection requirements, and the charge-signed rapidity difference is formed by the remaining lepton and the photon. No asymmetry is observed, as shown in Fig. 4.

VII. CONSISTENCY CHECKS

As a consistency check, the observed data is compared to the Standard Model photon E_T prediction. Figure 5 shows a plot of the overlay of the observed candidate photon E_T spectrum, the estimated background, and the expected Monte Carlo plus background distribution. The uncertainty on the candidate events is statistical, the background uncertainty is the corresponding uncertainty from the background estimate, and the Monte Carlo plus background error band includes the uncertainty from the background as well as the contribution from varying the acceptance, efficiencies, luminosity and cross section randomly within their uncertainties. The combined channel data distribution is consistent with the Standard Model plus background estimate with a χ^2 value of 20 for 17 degrees of freedom.

In addition, the cross section times branching ratio, $\sigma(p\bar{p} \rightarrow \ell\nu\gamma X)$, for events with photon $E_T > 7$ GeV, $\Delta R_{\ell\gamma} > 0.7$, and three-body transverse mass greater than 90 GeV/ c^2 is measured for both channels. The three-body transverse mass cut is used to enhance the contribution from prompt $W\gamma$ production. For the electron channel, the cross section times branching ratio is measured to be 3.12 ± 0.49 (stat. + sys.) ± 0.19 (lumi.) pb. For the muon channel, the cross section times branching ratio is measured to be 3.21 ± 0.49 (stat. + sys.) ± 0.20 (lumi.) pb. This is consistent with the Standard Model prediction of 3.21 ± 0.08 (PDF) pb.

VIII. RESULTS

Figure 6 shows the overlay of the charge-signed photon-lepton rapidity difference for the combined electron and muon channel candidate events, the background estimate, and the combined background plus Monte Carlo signal prediction. The uncertainties on the data are statistical. The error band about the Monte Carlo prediction plus background includes the systematic uncertainty on the background as well as the contribution from varying the acceptance, efficiencies, luminosity and cross section randomly within their uncertainties. The largest single contribution to the systematic uncertainty on the combined background comes from the $W + \text{jet}$ background. The largest single contribution to the systematic uncertainty on the combined Monte Carlo prediction comes from the uncertainty on the luminosity.

Figure 7 shows the background subtracted data overlaid with the Standard Model prediction. The uncertainties on the data points are statistical and systematic combined. The band is the systematic uncertainty on the signal Monte Carlo as described above. This result is consistent with the Standard Model prediction with a χ^2 of 16 for 12 degrees of freedom.

To measure the statistical significance of the dip that exists in the candidate distribution, the probability of the measured depletion of events in the expected region to be a statistical fluctuation is calculated. This is done by creating a histogram of the candidate events with three equal width bins that sample the events in the two peaks and the dip. The bins edges are chosen by using Standard Model Monte Carlo and are found to be at -2.8 , -1.2 , 0.4 , and 2.0 . See Figs. 8 and 9. Two ratios and their statistical uncertainties are calculated: one of the number of candidates in the middle bin to the number of candidates in the leftmost bin and the other of the number of candidates in the middle bin to the number of candidates in the rightmost bin. By calculating the probability for the ratios to be greater than or equal to 1, the unimodal hypothesis is ruled out at 90% confidence level. As a cross check, the dip test developed by Hartigan and Hartigan [9] is also utilized, and the probability of the dip is found to be in the range of 80% – 90%.

As a further test, the shape of the combined channel background subtracted distribution is compared to an alternative hypothesis as well as to the SM prediction. The alternative hypothesis is chosen from the set of anomalous $WW\gamma$ couplings which produce a zero magnetic dipole moment for the W boson. The couplings $\kappa_\gamma = -1$ and $\lambda_\gamma = 0$ are used and are theoretically expected to produce a unimodal distribution. For the test, the shape of the MC distribution is fixed, but the normalization is allowed to float to the value that minimizes the χ^2 test for the two distributions. The result of the test is shown in Fig. 10. The minimum χ^2 value for the alternative hypothesis is 9 for 11 degrees of freedom. The SM value is 15 for 11 degrees of freedom. For reference, a plot of the difference between the SM prediction and the distributions for the data and the anomalous coupling is shown in Fig. 11. It should be noted that the introduction of anomalous couplings will enhance the $W\gamma$ production cross section. If the test is repeated with the appropriate cross section normalization, then the result shown in Fig. 12 is obtained. The resulting χ^2 value for the alternative hypothesis is 55 for 12 degrees of freedom.

IX. CONCLUSION

The charge-signed rapidity distribution is consistent with the Standard Model prediction and has a shape indicative of the radiation amplitude zero. However, based on the shape-only information, it is not statistically inconsistent with the non-zero anomalous couplings case which correspond to the magnetic dipole moment of zero for the W , *i.e.* when the radiation zero is not expected theoretically. More statistics are required to unambiguously establish the radiation amplitude zero in $W\gamma$ production.

-
- [1] U. Baur, S. Errede and G. Landsberg, “Rapidity correlations in $W\gamma$ Production at Hadron Colliders,” *Phys. Rev. D* **50**, 1917 (1994) [arXiv:hep-ph/9402282].
 - [2] B. Abbott *et al.*, “Studies of WW and WZ production and limits on anomalous $WW\gamma$ and WWZ couplings,” *Phys. Rev. D* **60**, 072002 (1999).
 - [3] J. Ohnemus, “QCD Corrections to Diboson Production,” International Symposium on Vector Boson Interactions, edited by U. Baur, S. Errede, T. Müller, AIP Press (1996) p. 60
 - [4] DØ Collaboration, V.M. Abazov *et al.*, *Nucl. Instrum. and Methods A* **565**, 463 (2006).
 - [5] U. Baur and E.L. Berger, *Phys. Rev. D* **41**, 1476 (1990).
 - [6] T. Sjöstrand *et al.*, *Comp. Phys. Commun.* **135**, 238 (2001).
 - [7] S. Sengupta, “The W Boson Production Charge Asymmetry in the Muon Channel at $\sqrt{s}=1.96$ TeV”, DØ Note 4855, 2006.
 - [8] A. Askew, A. Lyon and G. Pawloski, “Measurement of the Charge Signed Photon-Lepton Rapidity Difference in $W\gamma$ Events”, DØ Note 5256, 2006.
 - [9] J.A. Hartigan and P.M. Hartigan, “The Dip Test of Unimodality”, *Annals of Statistics* **13**, 70-84 (1985).

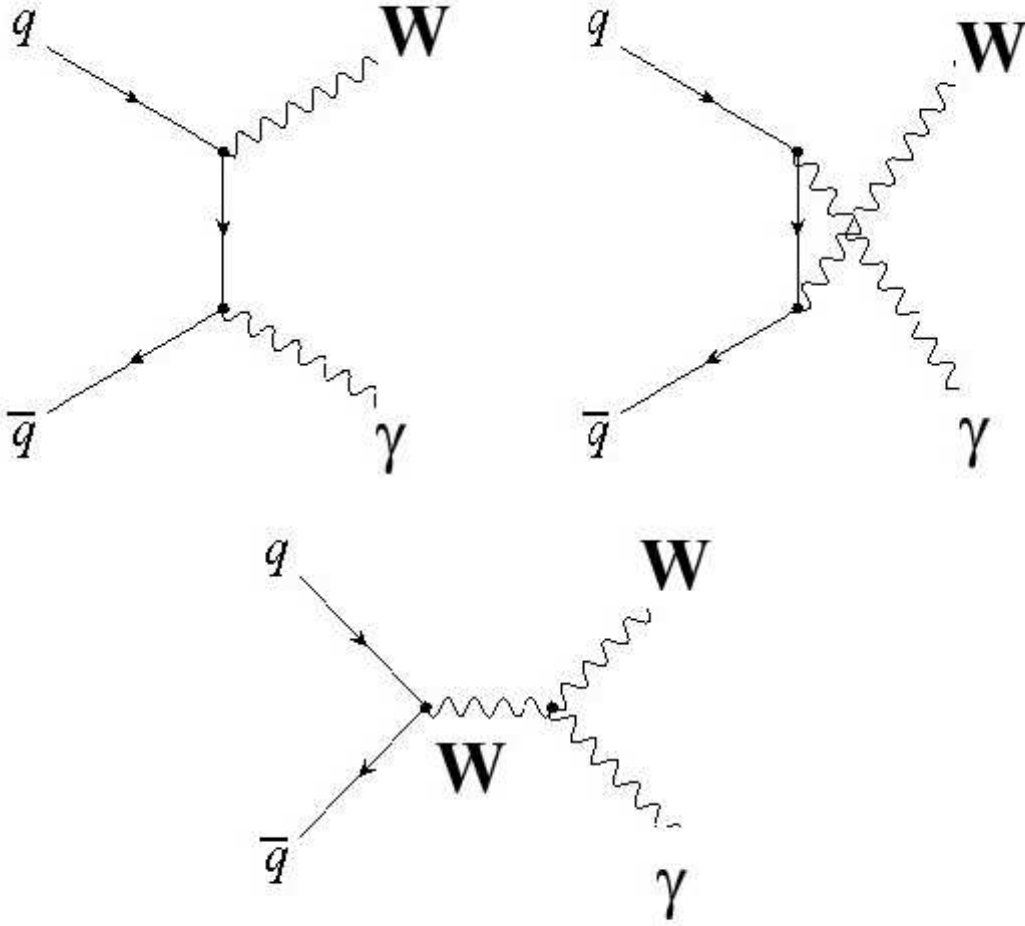


FIG. 1: Feynman Diagrams for $W\gamma$ production.

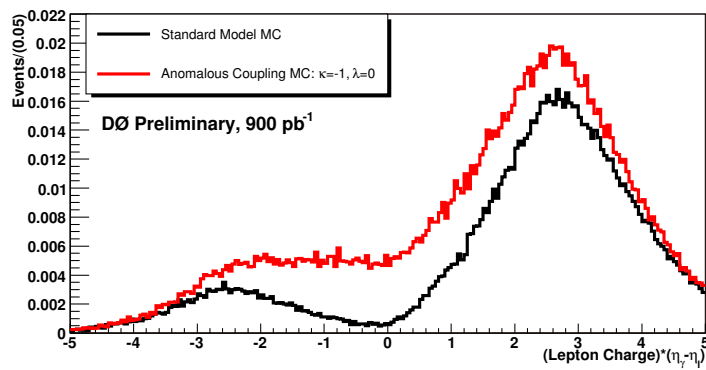


FIG. 2: MC prediction of the charge-sign rapidity difference for $W\gamma$ events. The $W\gamma$ events are required to have photon $E_T > 7$ GeV, $\Delta R_{\ell\gamma} > 0.7$, and three-body transverse mass greater than 110 GeV/ c^2 . The integral under each distribution has been normalized according to their respective cross sections with the SM integral being set to unity.

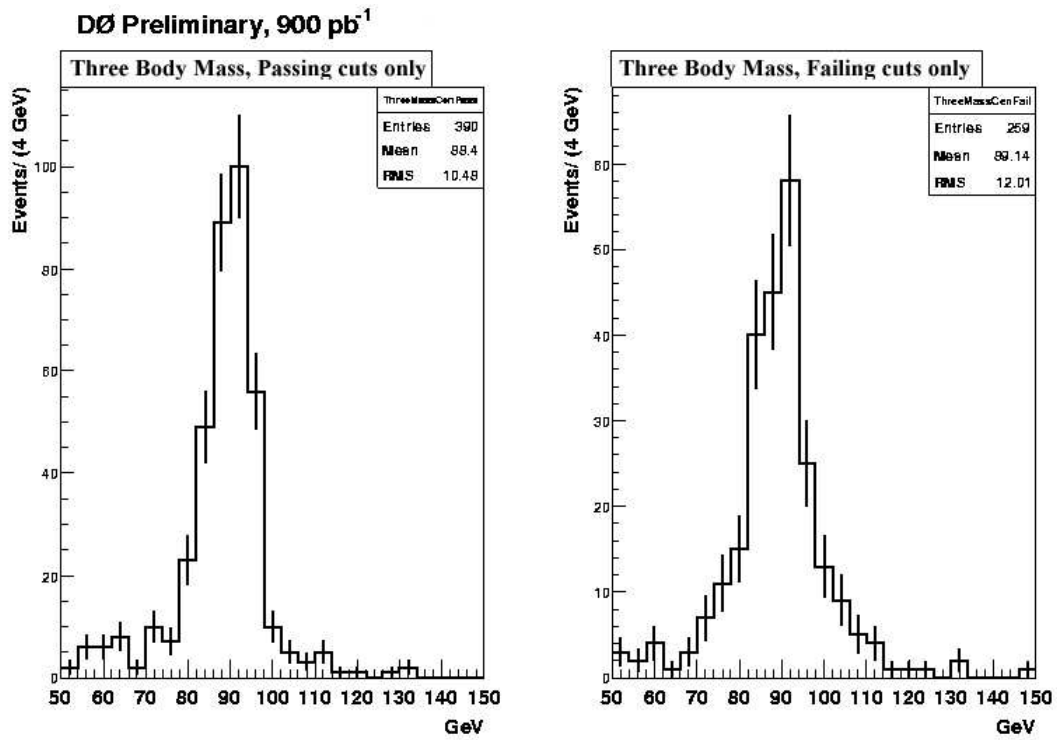


FIG. 3: Three-body mass peaks for radiative $Z\gamma \rightarrow \ell\ell\gamma$ events. The two peaks represent the samples passing all of the selection cuts, and those failing respectively.

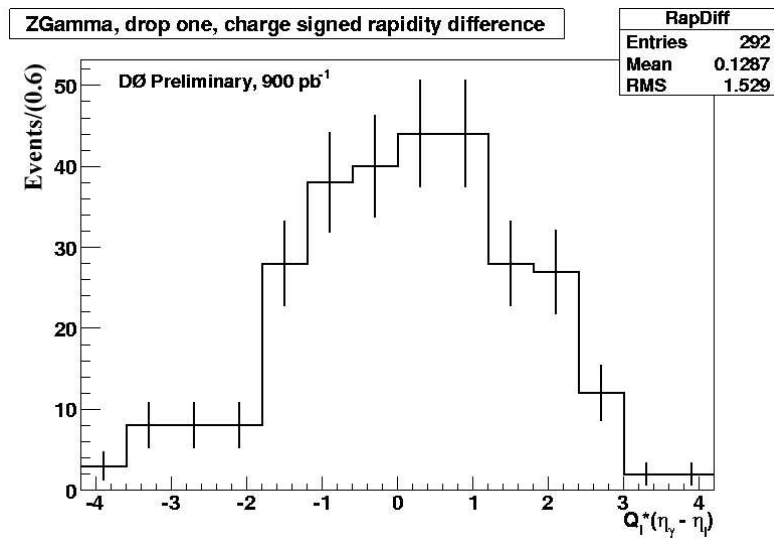


FIG. 4: Data charge-signed rapidity difference from $Z\gamma$ events.

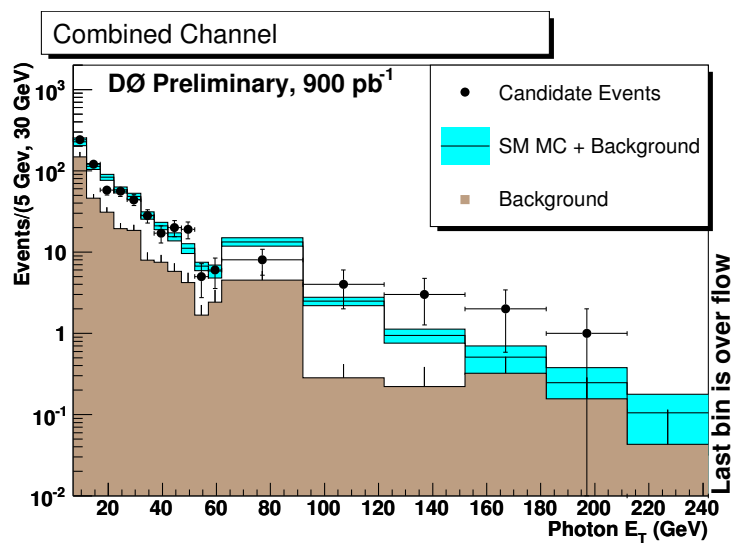


FIG. 5: Photon E_T of selected combined channel candidates.

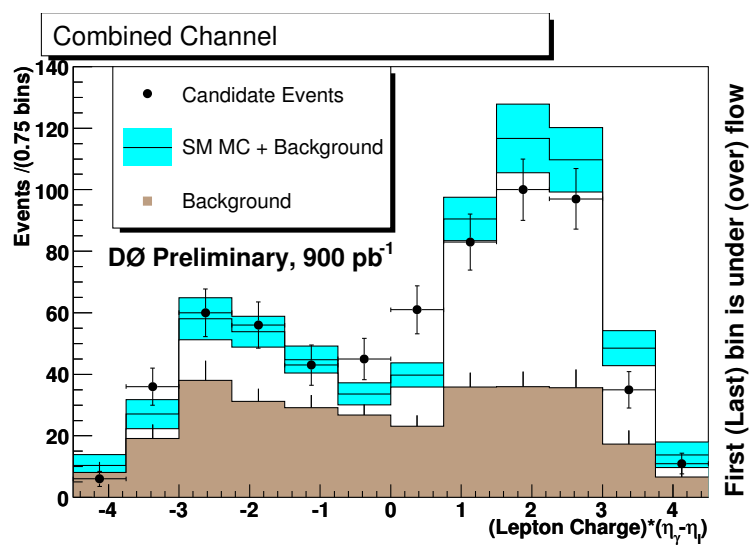


FIG. 6: Charge-signed rapidity difference of combined candidates.

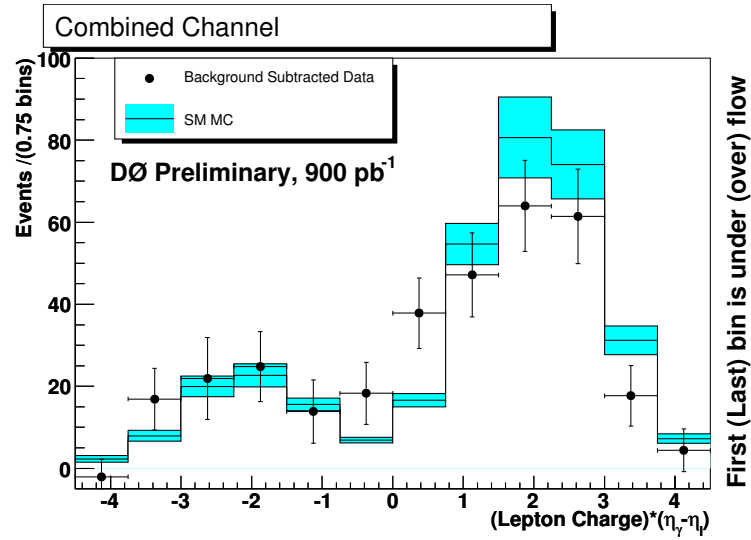


FIG. 7: Charge-signed rapidity difference of combined candidates, background subtracted.

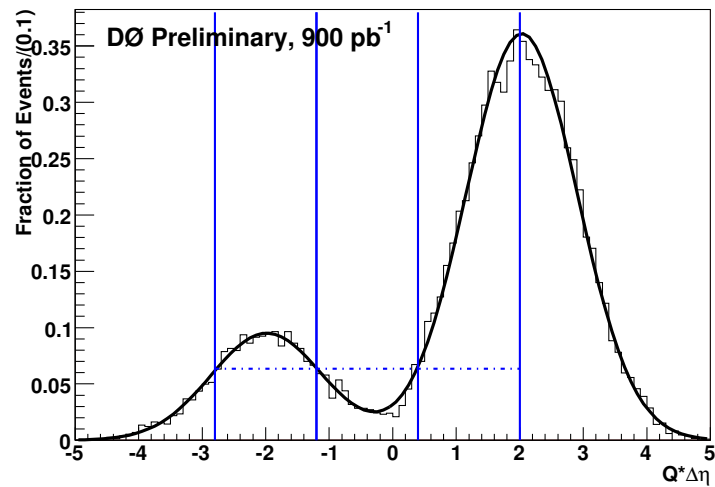


FIG. 8: Standard Model Monte Carlo of the charge-sign rapidity difference with detector effects. The integral under the distribution has been normalized to unity. The vertical lines represent the bin edges that are used for the dip test. The dashed line is simply a visual aid to demonstrate that all values of the fit in the bins that sample the peaks are greater than all values of the fit in the bin that samples the dip.

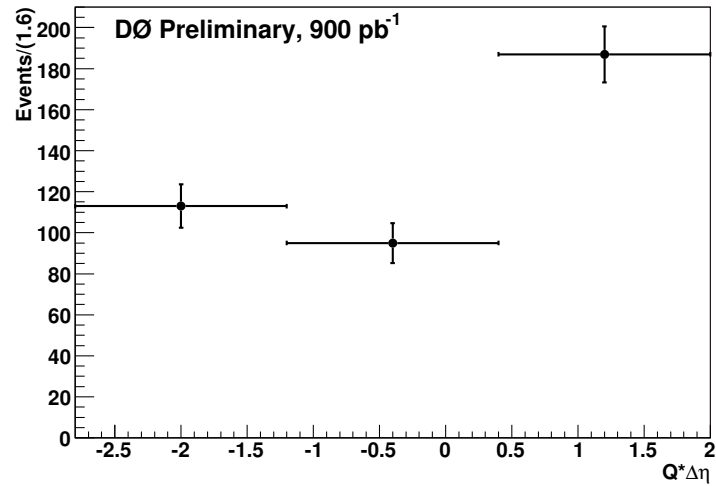


FIG. 9: Charge-sign rapidity difference of combined channel candidates used for the dip test.

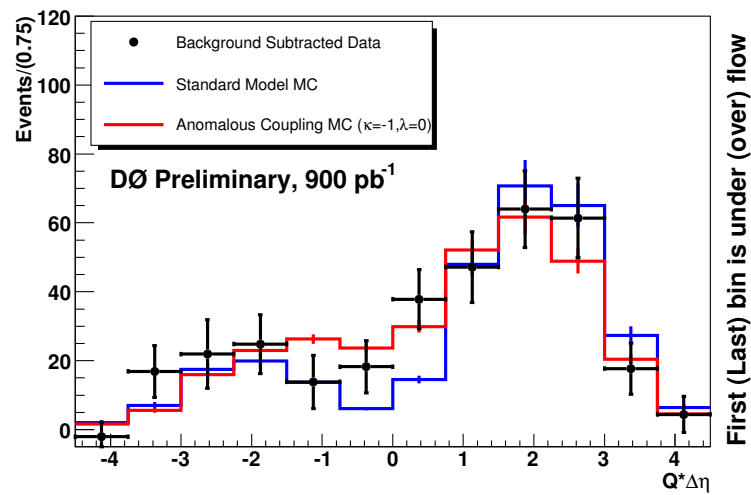


FIG. 10: Comparison of the shape of the SM distribution and an anomalous $WW\gamma$ coupling distribution to the background subtracted charge-sign rapidity difference for the combined channel candidates. The normalizations for the SM and anomalous coupling shapes are chosen from the best fits to the data.

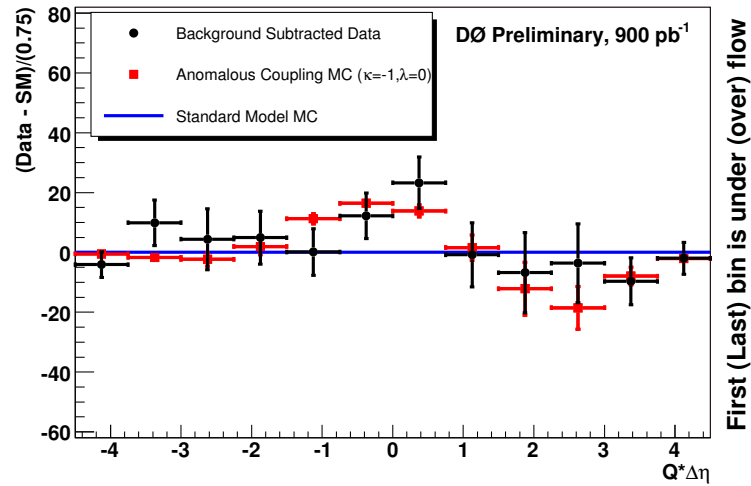


FIG. 11: The difference between the charge-sign rapidity distribution for the SM prediction and the distributions for the data and the anomalous coupling. The normalization for the SM and anomalous coupling shapes is chosen from the best fit of the SM shape to the data.

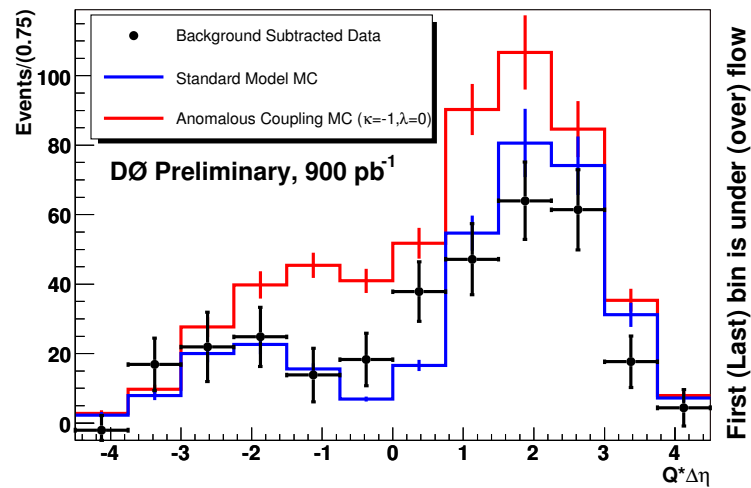


FIG. 12: Comparison of the SM distribution and an anomalous $WW\gamma$ coupling distribution to the background subtracted charge-sign rapidity difference for the combined channel candidates. The normalizations for the SM and anomalous coupling shapes are set by their respective cross sections.